Mon. Not. R. Astron. Soc. **304,** 595–610 (1999)

The 3D structure of the Virgo cluster from *H*-band Fundamental Plane and Tully–Fisher distance determinations

G. Gavazzi,[1⋆] A. Boselli,[2] M. Scodeggio,[3] D. Pierini[4] and E. Belsole[1]

[1]*Università degli Studi di Milano, Dipartimento di Fisica, via Celoria 16, 20133 Milano, Italy*
[2]*Laboratoire d'Astronomie Spatiale, BP8, Traverse du Syphon, F-13376 Marseille, France*
[3]*European Southern Observatory, Karl-Schwarzschild-Strasse 2, D-85748 Garching bei München, Germany*
[4]*Max-Planck-Institut für Kernphysik, Postfach 103980, D-69117 Heidelberg, Germany*

Accepted 1998 November 30. Received 1998 November 23; in original form 1998 April 23

ABSTRACT

We undertook a surface photometry survey of 200 galaxies in the Virgo cluster (complete to $B < 14.0$ mag) carried out in the near-infrared (NIR) H band. Combining velocity dispersion measurements from the literature with new spectroscopic data for 11 galaxies, we derive distances of 59 early-type galaxies using the Fundamental Plane (FP) method. The distances of another 75 late-type galaxies are determined using the Tully–Fisher (TF) method. For this purpose we use the maximum rotational velocity, as derived from H I spectra from the literature, complemented with new Hα rotation curves of eight highly H I-deficient galaxies. The zero-points of the FP and TF template relations are calibrated assuming the distance modulus of Virgo $\mu_0 = 31.0$, as determined with the Cepheids method. Using these 134 distance determinations (with individual uncertainties of 0.35 mag (TF) and 0.45 mag (FP)) we find that the distance of cluster A, associated with M87, is $\mu_0 = 30.84 \pm 0.06$. Cluster B, offset to the south, is found at $\mu_0 = 31.84 \pm 0.10$. This subcluster is falling on to A at about 750 km s^{-1}. Clouds W and M are at twice the distance of A. Galaxies on the north-west and south-east of the main cluster A belong to two clouds composed almost exclusively of spiral galaxies with distances consistent with A, but with significantly different velocity distributions, suggesting that they are falling on to cluster A at approximately 770 km s^{-1} from the far side and at 200 km s^{-1} from the near side respectively. The mass of Virgo inferred from the peculiar motions induced on its vicinity is consistent with the virial expectation.

Key words: galaxies: clusters: individual: Virgo – galaxies: fundamental parameters – galaxies: stellar content.

1 INTRODUCTION

Since the pioneering work of de Vaucouleurs (1961) the Virgo cluster, the nearest rich galaxy cluster in the Northern hemisphere, has been known to contain significant substructure. Clouds of galaxies were identified as independent units from the main M87 cluster, and they were suggested to lie at larger distances, purely on the basis of visual morphological classification. The deep photographic survey carried out by Binggeli, Sandage and Tammann (1985), with high scale plates, and the spectroscopic follow-up by Binggeli, Popescu and Tammann (1993), were major contributions to the understanding of the structure of the Virgo cluster. These works helped to establish that cluster A, containing M87, is separated from cluster B, dominated by M49, and that a number of individual clouds, namely clouds M, W, W′ and S (using de Vaucouleurs' designations), are separate entities.

Owing to their relative proximity, the distances to five galaxies in the Virgo cluster have been measured with the Cepheids method using ground-based observations (Pierce et al. 1994) or the *Hubble Space Telescope* (*HST*) (Ferrarese et al. 1996a; van den Bergh 1996; Saha et al. 1997). The distances of four of these (N4321, 4496, 4536 and 4571) were found to be consistent with 16 Mpc (corresponding to a distance modulus $\mu_0 = 31.0$), while the remaining one (N4639) was found at a larger distance of 25 Mpc ($\mu_0 = 32.0$) (Sandage et al. 1996; Saha et al. 1997). Distance determinations based on the Tully–Fisher (TF) relation (Tully & Fisher 1977) were used by a number of groups to infer the 3D structure of this cluster. Tully & Shaya (1984) and Pierce & Tully (1988) found evidence for a significant sample depth along the line of sight, interpreting their evidence as the presence of infall. Fukugita, Okamura & Yasuda (1993) used their photographic photometry to confirm that the cluster has a significant depth. More recently Yasuda, Fukugita & Okamura (1997) readdressed the issue, and concluded that the B, M and W clouds are at larger distances than Virgo itself. Federspiel,

⋆ E-mail: giuseppe.gavazzi@uni.mi.astro.it

Tammann & Sandage (1998) used new B-band photometry to pursue the issue. They agree with Yasuda et al. (1997) in determining that W and M are distant clouds. They confirmed that cluster B is 0.5 mag further away than Virgo itself, although the mean recessional velocity of this subcluster is identical to that of the dominant cluster A (Binggeli et al. 1993).

Beside the Cepheids and the TF relation, other methods have been used to estimate distances to the Virgo spirals. These include the peak of the luminosity versus declining ratio of Novae (Ferrarese et al. 1996b), the expanding photosphere method for the Type II supernovae (Schmidt et al. 1994), the peak brightness of the Type Ia supernovae (Schank 1997) and the bright stars as standard candles (Pierce, McClure & Racine 1992) methods. The mean distance modulus derived from these methods is 30.92 ± 0.28.

Distance estimates to early-type galaxies have been based on the surface brightness fluctuation method (Tonry, Ajhar & Luppino 1990; Jensen, Luppino & Tonry 1996; Morris & Shanks 1998; Ajhar et al. 1997), on novae luminosities (Della Valle & Livio 1995), on the globular clusters luminosity function (Secker & Harris 1993; Whitmore et al. 1995; van den Bergh 1996), and on the planetary nebulae luminosity function (Jacoby, Ciardullo & Ford 1990; Ciardullo et al. 1998). These methods give distances in the range 30.31–32.13. M87 itself has been found at $\mu_0 = 30.8$–31.3. M49 poses a problem, since its distance determination ($\mu_0 = 31.0$) is significantly smaller than the distance estimate to cluster B ($\mu_0 = 31.8$, Federspiel et al. 1998) to which it is supposed to belong.

Altogether there appears to be unanimous consent that galaxies in the Virgo region are not at a unique distance. The W, M and B clouds are found to be further away than A, and evidence for infall has been reported.

In this paper we make a further step in the direction of unveiling the structure of the Virgo cluster, with two main improvements over previous works. First, we combine distances to spirals obtained with the TF method with distances to E/S0s obtained with the Fundamental Plane (FP) method (Djorgovski & Davis 1987; Dressler et al. 1987), thus increasing the statistical significance of the determination. Secondly, for both of these methods we rely on H-band surface photometry. The advantages of using near-infrared (NIR) photometry over the B band are that NIR magnitudes are less sensitive to recent episodes of star formation, and they are less affected by internal extinction, thus they better trace the luminous matter in galaxies (Gavazzi, Pierini & Boselli 1996b). Also, spiral discs have a smoother appearance in the NIR, and this makes it easier to fit photometric profiles to derive the galaxy total magnitude, and the disc inclination. Both these factors should contribute to a reduction in the overall uncertainty with which distance determinations are obtained.

The remainder of this paper is organized as follows. In Section 2 we illustrate the sample selected for the present analysis. The H-band imaging observations and the new spectroscopy are briefly summarized in Section 3. The cosmological assumptions, and the derivation of the TF and FP templates are described in Section 4. Our new distance estimates, and a comparison with other estimates from the literature, are presented in Section 5, together with a discussion on the structure of the Virgo cluster as delineated by these new measurements. Our main conclusions are summarized in Section 6.

2 THE SAMPLE

Galaxies analysed in this work are selected from the 220 Virgo Cluster Catalog (VCC; Binggeli et al. 1985) objects with $B < 14.0$. We add to this sample 13 objects, slightly fainter than this limit, that were taken from the CGCG catalogue (Zwicky et al. 1961–68), because distance estimates are readily available for them. For each galaxy a membership estimate is given in the VCC (revised by Binggeli et al. 1993). Cluster A coincides with the X-ray cluster associated with M87. The subcluster B is centred on M49. Other aggregates include the M, W and W′ clouds and the Southern extension. Galaxies with $V_{\rm hel} > 3000$ km s^{-1} are treated as background objects, and are excluded from the present analysis.

Both the availability of the photometric and spectroscopic data necessary to build the TF and FP relation, and inclination restrictions that apply to any TF sample, play a role in limiting the number of galaxies for which we can obtain distance estimates. We have obtained NIR H- or K'-band images of 200 out of the 233 selected galaxies (these observations are described in Section 3). Of the 89 early-type galaxies imaged, 48 have central velocity dispersion measurements available in the literature (McElroy 1995). To these we add 11 new measurements of the central velocity dispersion obtained at the OHP (see Section 3.4).

Of the 111 spiral galaxies imaged, 75 match the criteria for the inclusion in the TF sample, i.e. (a) have the correct inclination ($i > 30°$) (see Section 4.2), (b) have high signal-to-noise ratio 21-cm H I line profiles (or Hα rotation curves), and (c) meet the additional requirement that the linewidths corrected for inclination exceed 100 km s^{-1}). The H I line profiles in the literature were individually inspected. If more than one measurement was available, we chose the one with higher signal-to-noise ratio (references to these measurements are listed in Table 2).

NGC 4496, one of the five galaxies with Cepheids measurements, is not included in the present analysis because another galaxy is superimposed on its disc, making the extraction of its photometric parameters uncertain. Conversely, two other galaxies with Cepheids (NGC 4321 and 4571) are included in the present work in spite of their low inclination (27°).

3 OBSERVATIONS

3.1 NIR imaging observations

In various runs from 1994 to 1997 we took NIR H- (1.65-μm) or K'- (2.1-μm) band images of 206 of the 233 galaxies selected from the VCC and CGCG, using the TIRGO 1.5-m and the Calar Alto 2.2-m telescopes. Eight galaxies were not observed because they have velocity larger than 3000 km s^{-1}, thus they do not belong to the cluster, and four because their angular size ($a > 4$ arcmin) exceeds that of the available NICMOS3 detectors. The remaining 15 objects were not observed because of time limitations. Images of six galaxies are not usable, because the frames were ruined by stray light from the Moon. Of the 200 images available, 166 were taken in H band, and 34 in K' band. The K' data are converted into H band using $\langle H - K' \rangle = 0.25 \pm 0.13$ mag. This colour, based on 425 measurements not all included in this work, depends little on morphological type (0.24 for E+S0; 0.27 for S+Irr).

3.2 Calar Alto observations of late-type galaxies

NIR images are available for 111 late-type galaxies: 83 at H band and 28 at K' band. The K'-band observations (and 19 of the H-band ones) were taken in 1994–1996 with the Calar Alto 2.2-m telescope, and are published in Boselli et al. (1997). H-band observations of 15 late-type galaxies were taken in 1995 with the

TIRGO 1.5-m telescope, and are published in Gavazzi et al. (1996a).

Images in the H band for the remaining 49 galaxies were obtained during three photometric nights of 1997 February with the Calar Alto 2.2-m telescope, in seeing conditions of typically 1–2 arcsec. The Cassegrain focus of the telescope was equipped with the MAGIC 256×256 pixel NICMOS3 infrared array (Herbst et al. 1993) with an optical setup of the detector chosen to give the largest possible field of view, i.e. 6.8×6.8 arcmin^2, with a pixel size of 1.61 arcsec. The observing technique was identical to that used in previous K'-band observations of late-type galaxies at Calar Alto, as described in Boselli et al. (1997).

Galaxies with optical diameter larger than half of the size of the field of view of the array were observed using a pointing sequence in which eight frames are taken, centred on the target, alternated with eight sky frames, positioned along a circular path around the galaxy (offset by a field of view from the centre). The eight on-target fields were dithered by 10 arcsec in order to help the elimination of bad pixels.

Galaxies with optical diameter smaller than half of the size of the field of view of the array were observed with a pointing sequence consisting of nine pointings along a circular path and displaced from one another by 2 arcmin such that the target galaxy is always in the field. Galaxies with angular sizes larger than the dimension of the detector were mapped using pointing sequences expressly prepared according to the shape and orientation of the galaxy in the sky, in order to cover with a mosaic the entire surface of the target.

Typical integration times were 256–288 s. This corresponds to the product of the exposure time of the elementary integration (1 s), the number of elementary integrations (32) and the number of pointings used in each mosaic (8 or 9).

The observations were calibrated and the fluxes transformed into the H-band photometric system using the standard stars in Elias et al. (1982), observed hourly throughout the night. The typical uncertainty of the measurements is 0.05 mag.

Details on the image analysis and extraction of the photometric parameters can also be found in Boselli et al. (1997). Here it is sufficient to say that the H magnitudes used in the present analysis were derived by simulating aperture photometry, following the method of Gavazzi & Boselli (1996): the counts are integrated in concentric circular rings around the galaxy centres to provide curves of growth up to the galaxy optical diameter (determined in the B at the 25th mag arcsec^{-2}). The H magnitudes used in this work are corrected for internal extinction using the prescriptions of Gavazzi & Boselli (1996). For 1053 galaxies (not necessarily included in this work) for which an image is available in H band we compare the corresponding H magnitudes with those obtained by de Vaucouleurs plus exponential decomposition of the light profiles obtained along elliptical annuli. We find that on average H are 0.10 ± 0.21 mag fainter than the total (extrapolated to infinity) magnitudes.

3.3 TIRGO observations of early-type galaxies

NIR images are available for 89 early-type galaxies: 83 at H band, and six at K'-band. The K' band observations were taken with the Calar Alto 2.2-m telescope, and are published in Boselli et al. (1997).

The H-band observations were carried out with the TIRGO 1.5-m telescope at Gornergrat equipped with the NICMOS3 camera ARNICA (Lisi, Baffa & Hunt 1993; Lisi et al. 1996) on 22 nights from 1997 March 13 to April 13, as part of an extensive survey of early-type galaxies in the Virgo cluster, which will be described elsewhere (Gavazzi et al., in preparation). The optical setting of the camera provides a field of view of 4.3×4.3 arcmin^2, with 0.96-arcsec pixels. The average seeing was 2.3 arcsec. The observing technique was similar to that used for the Calar Alto observations, and also in previous observations at TIRGO of late-type galaxies, as described in Gavazzi et al. (1996a), and of early-type galaxies in the Coma cluster, described in Scodeggio et al. (1998a). Here we briefly summarize some of the observing parameters relevant to this work. All galaxies with apparent B diameter > 1.0 arcmin were observed with pointing sequences that consist of eight frames centred on the source, alternated with eight sky frames, positioned along a circular path around the source and offset by 4 arcmin. The on-source positions were dithered by 10 arcsec to improve the flat-fielding, and to facilitate bad pixel removal. The total integration time was 384 s, both for the target galaxy and for the sky frames. Galaxies with apparent B diameter < 1.0 arcmin were observed with sequences of nine pointings along a circular path, displaced from one another by 1 arcmin, such that the target galaxy was always in the field. The total integration time was 432 s. The data were calibrated with standard stars in the Elias et al. (1982) catalogue, with a typical photometric uncertainty of 0.05 mag. We checked our photometric calibration against 560 aperture photometry H-band measurements available in the literature for 178 galaxies. Agreement was found within 0.10 mag, which we thus take as the photometric accuracy of the present investigation.

The basic image reduction was performed using standard routines in the IRAF–STSDAS–PROS environment.[1] The bias-subtracted, flat-fielded, combined and calibrated images were analysed using the package GALPHOT (developed for IRAF–STSDAS mainly by W. Freudling, J. Salzer and M. Haynes, and adapted by one of us (MS) to perform the light decomposition of early-type galaxies). For each frame the sky background was determined as the mean number of counts measured in regions of 'empty' sky, and it was subtracted from the frame. Sky-subtracted frames were inspected individually and the light of unwanted superposed or nearby stars and galaxies was masked. The 2D light distribution of each galaxy was fitted with elliptical isophotes, using a modified version of the STSDAS ISOPHOTE package. The fit maintains as free parameters the ellipse centre, ellipticity and position angle, and the ellipse semimajor axis is incremented by a fixed fraction of its value at each step of the fitting procedure. Using the fitted parameters a model of the galaxy light distribution is obtained, which is used to compute integrated magnitudes as a function of semimajor axis.

The effective radius r_e and effective surface brightness μ_e (the mean surface brightness within r_e) of each galaxy were obtained by fitting its radial surface brightness profile with a de Vaucouleurs $r^{1/4}$ law (de Vaucouleurs 1948). The fit was performed from a radius equal to twice the seeing radius, out to the outermost isophotes for E galaxies; for S0 and S0a galaxies only the central core was fitted. The median uncertainty on the determination of $\log r_e$ and μ_e is 0.05 and 0.16 mag, respectively.

[1] IRAF (Image Reduction and Analysis Facility) is distributed by NOAO, which is operated by the Association of Universities for Research in Astronomy, Inc. (AURA), under cooperative agreement with the National Science Foundation. STSDAS (Space Telescope Science Data Analysis System) is distributed by STScI, which is operated by AURA, under contract to the National Aeronautics and Space Administration.

3.4 Long-slit spectroscopy

To obtain high-dispersion spectra of 21 target galaxies we used the 1.93-m telescope of the Observatoire de Haute Provence (OHP), equipped with the Carelec spectrograph (Lemaitre et al. 1990) coupled with a 512×512 pixel Tektronix charge-coupled device (CCD). The observations were carried out in the nights of 1998 February 26–March 5, in 2–2.5 arcsec seeing conditions. The spatial resolution is 1.17 arcsec/pixel^{-1}. The slit was 1.83 arcsec wide. We used two grisms, both with a spectral resolution of 33 Å mm^{-1}.

The red grism was chosen to give a spectral coverage in the region 6475−6930 Å, containing the redshifted Hα (λ6562.8), the [N II] doublet ($\lambda\lambda$6548.1, 6583.4) and the [S II] doublet ($\lambda\lambda$6717.0, 6731.3). This setup was selected to obtain Hα rotation curves of 11 spiral galaxies with large (> 0.7) H I deficiency. Each galaxy was observed with the slit parallel to the major axis, with an integration time of 15 min, ensuring a signal-to-noise ratio of ∼10–15 per pixel at Hα. For three of these objects (70099, 70115, 70149) the Hα was instead detected in absorption along with the [Ca I] (λ6492.5), providing us with a useful velocity dispersion measurement.

The blue grism was selected to give a spectral coverage in the region 5050−5505Å, containing the redshifted [Mg I] triplet ($\lambda\lambda$5167.3, 5172.7, 5183.6) and the CaFe doublet (λ5269.0). With the blue grism we obtained dispersion measurements of 10 early-type galaxies. Each galaxy was observed with the slit positioned east–west, with an integration time varying from 20 to 45 min, depending on the brightness of the galaxy, enough to produce a signal-to-noise ratio of ∼15 per pixel at [Mg I]. Each observation was preceded by an exposure of an Ar lamp to ensure the wavelength calibration. The calibration was checked using known sky lines, which were found within 0.1 Å from their nominal wavelengths. The estimated redshift uncertainty is 10 km s^{-1}.

The rotation curves of eight galaxies were obtained by determining the central wavelength of a Gaussian fit, pixel per pixel along the slit, to the redshifted Hα. These are given in Fig. 1 and their parameters are listed in Table 1.

The velocity dispersion measurements of 13 galaxies were obtained using the Tonry & Davis (1979) method. This method is based on a 'comparison' between the spectrum of a galaxy whose velocity dispersion is to be determined, and a fiducial spectral template of a star of appropriate spectral type to contain the wanted absorption lines. The basic assumption behind this method is that the spectrum of an elliptical galaxy (and also of the bulge of a disc galaxy) is well approximated by the spectrum of its most luminous stars (K0–K1 giants), modified only by the effects of the stellar motions inside the galaxy. We observed three stars of K type, HD 26162, 132737 and HR 5361, with integration time of 60 s, to secure a spectrum with sufficient signal-to-noise ratio. The heliocentric velocities of these stars are known within a few km s^{-1} accuracy. The quantitative measurements of the spectra have been obtained using the cross-correlation technique of Tonry & Davis (1979), implemented in the IRAF task FXCOR (for more details on the application of this technique see Scodeggio 1997). Since the velocity dispersion inside an elliptical galaxy varies as a function of radial distance from the centre, we extracted from our data 1D spectra of the central 6 arcsec. The measurements were then corrected to the value that one would obtain at the distance of the Coma cluster, using the relation derived by Jørgensen, Franx & Kjærgaard (1996):

$$\log(\sigma/\sigma_{6''}) = +0.04 \log(d_{\rm Virgo}/d_{\rm Coma}),$$

where $\sigma_{6''}$ and σ are the measured and corrected velocity dispersion, and $d_{\rm Virgo}$ and $d_{\rm Coma}$ are the respective distances, assumed to be 16 and 88.3 Mpc. The velocity dispersion measurements obtained in this work are listed in column 7 of Table 3 along with their internal errors. The total uncertainty can be obtained by adding in quadrature the systematic uncertainty of 10 km s^{-1}. Unfortunately two of the newly obtained dispersion measurements (42026 and 70100) are not used in the present analysis because these galaxies have no *H*-band surface photometry.

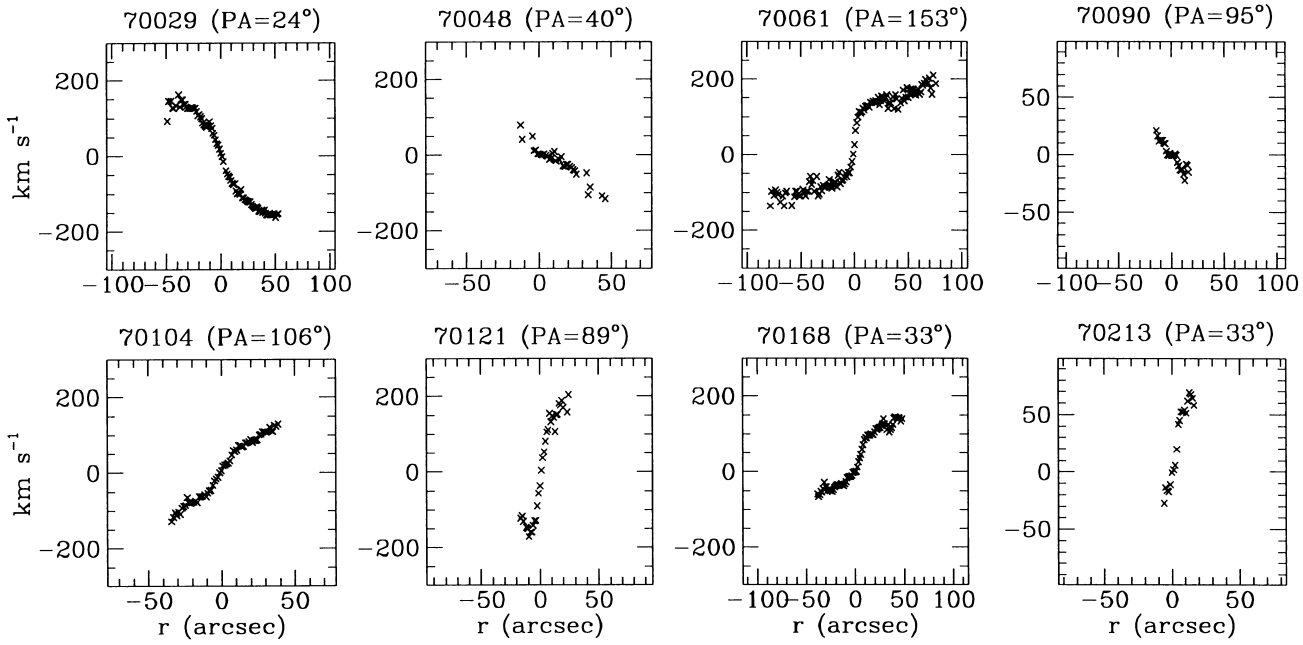

Figure 1. The rotation curves of eight H I-deficient galaxies observed at the OHP. The extent of the horizontal scale is up to the galaxy optical diameter. Galaxies 70048, 70090 and 70213 are not used in the following analysis.

3.5 The Tully–Fisher parameters of H I-deficient galaxies

Some 22 spiral galaxies included in the present analysis have exceedingly large (> 0.7) H I deficiency that could produce systematic underestimates of their widths, thus of their TF distances. We inspected these H I profiles individually and we searched in the literature for alternative maximum rotational velocity measurements, either from CO observations (Kenney & Young 1988; Thronson et al. 1989; Boselli, Casoli & Lequeux 1995; Kenney et al. 1995) or from Hα rotation curves (Chincarini & de Souza 1985; Speraindio et al. 1995; this work). Table 1 reports detailed information on the rotational properties of these galaxies, as follows:

Columns 1–3: CGCG, NGC, VCC designations.

Column 4: Morphological type as given in the VCC.

Column 5: H I deficiency parameter as defined by Haynes & Giovanelli (1984).

Column 6: Logarithm of the maximum rotational velocity, corrected for inclination, as derived from H I observations (average of 20 per cent and 50 per cent of the peak value).

Column 7: A quality mark given to each H I profile after individual inspection: 1 are two-horn, high S/N profiles; 2 are one-horn, high S/N profiles; 3–4 are profiles of insufficient quality for TF work.

Column 8: Galaxy inclination in the plane of the sky (determined following Haynes & Giovanelli 1984).

Column 9: Reference to the H I data.

Columns 10–12: Logarithm of the maximum rotational velocity, corrected for inclination, as derived from CO observations or Hα rotation curves, with references.

If the three available measurements are found to be in agreement, we use the H I maximum linewidths. Alternatively we use combinations of CO and Hα measurements (when both are available, as for 99054 and 70097) or we adopt the Hα values alone, if the data extend sufficiently to ensure that the plateau of the rotation curve is reached.

For three galaxies (70048, 70090 and 70213) observed in this work the Hα data do not trace the rotation curve far enough to see the classical S shape, indicative that the plateau of the rotation curve has been reached. Their Hα maximum rotational velocity is smaller than that obtained from the H I line (although of poor quality). These galaxies have been omitted from the analysis.

One object (70104) has a rotaton curve with marginal change of concavity. However, its maximum velocity determination exceeds that available from the H I profile. We decided to rely on the Hα measurement. The remaining four objects observed at OHP show a clear S-shaped rotation curve. For these we adopt the maximum velocity obtained from our Hα measurement.

4 THE METHOD

We assume that the average distance of the Virgo cluster A (membership is taken from Binggeli et al. 1993) is 16 Mpc ($\mu_0 = 31.02$), as derived from recent primary distance determinations of four *HST* galaxies with Cepheids (van den Bergh 1996). We also assume that the difference of distance moduli between Virgo cluster A and Coma is 3.71 mag; thus $\mu_{0\,\mathrm{Coma}} = 34.73$ or $D_{\mathrm{Coma}} = 88.3$ Mpc (van den Bergh 1996).

Given that the average recessional velocity of Coma corrected for the motion with respect to the cosmic microwave background (CMB) is $\langle V\rangle_{\mathrm{CMB}} = 7185$ km s^{-1} (Giovanelli et al. 1997), the previous assumptions imply $H_0 = 81.35$ km s^{-1} Mpc^{-1}.

The infall velocity of the Local Group (LG) towards Virgo is taken to be 220 km s^{-1} (see Federspiel et al. 1998); velocities with respect to LG centroid, V_{LG}, are thus computed as $V_{\mathrm{hel}} + 220$.

Distances to Virgo cluster early- and late-type galaxies are computed using the FP and TF relation, respectively. Templates for these

Table 1. Dynamical parameters of H I-deficient galaxies.

CGCG (1)	NGC (2)	VCC (3)	T (4)	$\mathrm{Def_{H\,I}}$ (5)	$\log W_{\mathrm{cH\,I}}$ (6)	Qual (7)	i (8)	Ref[a] (9)	$\log W_{\mathrm{c}}$ (10)	From (11)	Ref[a] (12)	Comment (13)
99029	4312	559	Sab	1.24	2.35	1	78.3	HH84	2.35	H I	HH84	
70034	4313	570	Sab	1.09	2.44	1	77.7	HH84	2.44	H I	HH84	
70039	4330	630	Irr	0.90	2.44	1	76.6	HH84	2.44	H I	HH84	
70068	4388	836	Sab	0.83	2.60	1	78.8	HG81	2.60	H I	HG81	
70076	4413	912	Sbc	0.76	2.33	1	48.1	HG81	2.38	CO	B95	
99054	4419	958	Sa	1.05	2.43	1	72.5	GK83	2.62	⟨Hα, CO⟩	S95-KY88	
70097	4438	1043	Sb	1.25	2.43	2	67.4	GK83	2.67	⟨Hα, CO⟩	CS85-K95	
99062	4450	1110	Sab	0.87	2.66	1	44.7	HH84	2.66	H I	HH84	
99065	I3392	1126	Sb	1.05	2.35	1	63.9	HL89	2.35	H I	HL89	
42124	4457	1145	Sb	0.83	2.48	2	34.3	GK83	2.50	CO	T89	
99090	I800	1532	Sc	0.72	2.23	2	40.9	HG86	2.23	H I	HG86	
70192	4569	1690	Sab	1.20	2.62	1	62.8	CG90	2.68	Hα	CS85	
70197	4579	1727	Sab	0.81	2.84	1	36.5	CG90	2.84	H I	CG90	
42187	4586	1760	Sa	1.08	2.44	1	72.5	HH84	2.44	H I	HH84	
70029	4307	524	Sbc	1.35	2.60	3	77.8	HH84	2.52	Hα	T.W.	
70061	4380	792	Sab	0.89	2.55	1	54.5	HH84	2.63	Hα	T.W.	
70104	4445	1086	S	1.26	2.37	4	90.0	HL89	2.41	Hα	T.W.	
70121	4469	1190	Sa	>1.76	–	0	71.9	GK83	2.59	Hα	T.W.	
70168	4522	1516	Sbc	0.76	2.37	1	73.8	HH84	2.34	Hα	T.W.	
70048	4356	713	Sc	1.24	2.47	3	83.0	HG86	2.30	Hα	T.W.	(not used)
70090	4424	978	Sa	1.09	1.95	2	61.9	GK83	1.75	Hα	T.W.	(not used)
70213	4606	1859	Sa	1.63	2.36	3	58.2	HH84	2.09	Hα	T.W.	(not used)

[a] See footnote *b* to Table 2 for a listing of references.

relations are obtained from other well-studied clusters, scaling to the appropriate distances on the basis of the above assumptions.

4.1 The Fundamental Plane relation

An H-band FP template was derived from a sample of 74 galaxies in the Coma cluster by Scodeggio et al. (1998a). The best fit to this relation, obtained assuming that Coma is at rest in the CMB reference frame (see, for example, Giovanelli et al. 1997; Scodeggio, Giovanelli & Haynes 1997), is $\log R_e = -8.354 + 1.52 \log \sigma + 0.32 \mu_e$ (with the zero-point adapted to $H_0 = 81.35$). The scatter of the template relation, thus the uncertainty on the distance modulus determination of a single galaxy, is 0.45 mag.

The fit is obtained by minimizing the weighted sum of the orthogonal distances of the data points from the plane. This is a generalization to three dimensions of the maximum-likelihood method of Press et al. (1992) (their FITEXY routine), with a modification introduced to take into account the high degree of covariance shown by the uncertainties on the determination of log R_e and μ_e (see Scodeggio 1997 for details). Uncertainties on the FP parameters are determined using the statistical jack-knife: N subsamples, each one composed of $N - 1$ data points, are extracted from the original sample of N data points, rejecting in turn one of the data points. The distribution of a certain statistical parameter among those N subsamples is then used to estimate the uncertainty in the value of that same parameter, without having to assume an a-priori statistical distribution for the parent population of the data set under examination (see for example Tukey 1958; Efron 1987).

The FP relation of early-type Virgo galaxies is given in Fig. 2(a) superposed to the fit of the Coma template relation. The points are coded according to whether σ is larger or smaller than 100 km s^{-1}. It is known that uncertainties in the measurement of such low velocity dispersions are larger than in the case of galaxies with higher velocity dispersion (e.g. Scodeggio, Giovanelli & Haynes 1998b). In fact the dispersion of Virgo galaxies around the template relation is 0.75 mag if $\sigma < 100$ are excluded, significantly larger than that of the template relation. If these 12 galaxies are included, the dispersion rises to 0.85 mag, enough to suggest dropping galaxies with $\sigma < 100$ from the following analysis.

4.2 The Tully–Fisher relation

The TF template was derived by combining 73 galaxies from the clusters A262, Cancer, Coma and A1367. The clusters were considered to be at rest in the CMB reference frame. The galaxies were selected from the CGCG (Zwicky et al. 1961–68) (thus with

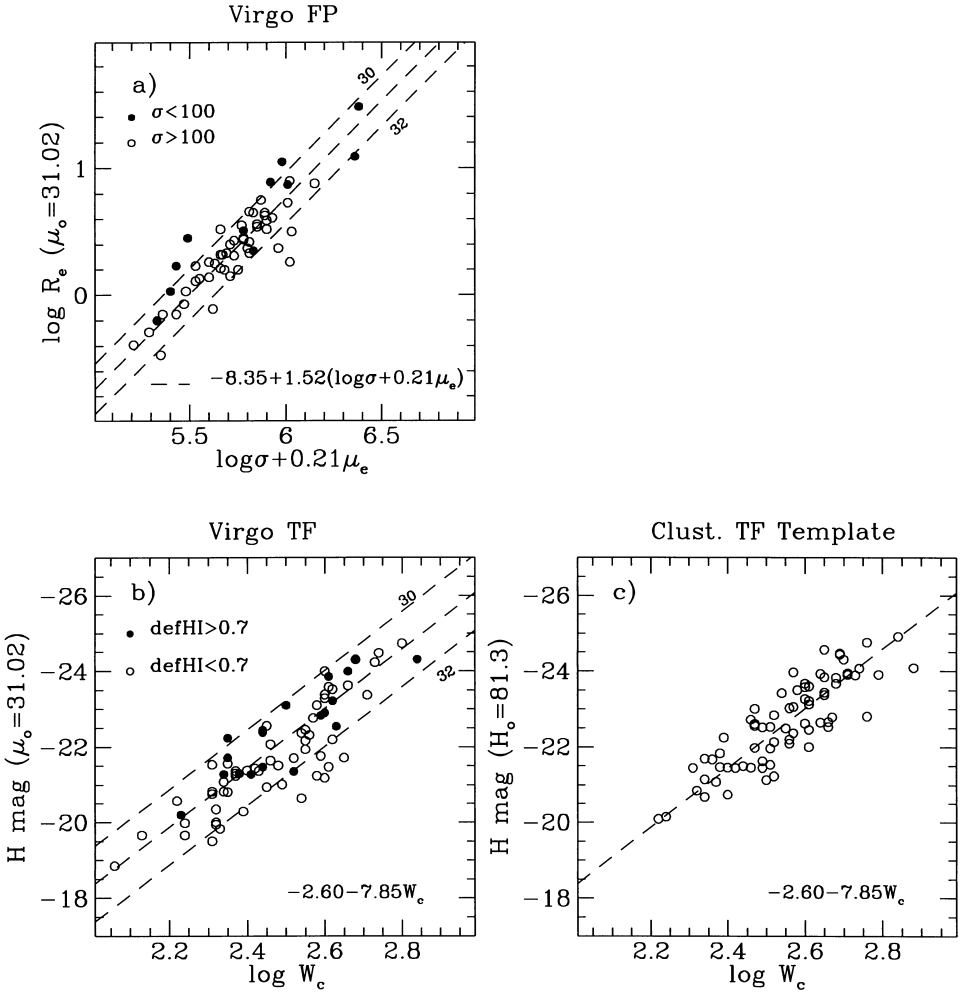

Figure 2. (a) The FP relation for 59 Virgo galaxies (dots) separated into $\sigma < 100$ and $\sigma > 100$ km s^{-1}. The template relation obtained on the Coma cluster is given using $\mu_0 = 31.0$ and ± 1 mag. (b) The TF relation for 75 Virgo galaxies (dots) separated into $\mathrm{Def_{H_I}} < 0.7$ and $\mathrm{Def_{H_I}} > 0.7$. The template relation obtained on four clusters is given using $\mu_0 = 31.0$ and ± 1 mag. (c) The 73 galaxies in the A262, Cancer, Coma and A1367 clusters used to derive a template TF relation.

$m_p \leq 15.7$) according to slightly more restrictive criteria than for the Virgo galaxies. *H*-band data for these galaxies were obtained from Gavazzi & Boselli (1996), while the 21-cm H I line data were collected from a large number of sources. It is important to stress here that the method used for determining the *H* magnitudes of the template galaxies is identical to that used for the Virgo galaxies (see Section 3.2). Galaxies with $\mathrm{Def}_{\mathrm{H\,I}} > 0.5$ were not used, because the H I linewidth in this case could underestimate the galaxy true rotation velocity. Also galaxies with $\log W_c < 2.2$ were not used, to avoid objects whose correction for turbulent motion is relevant. We assume that the uncertainty on the measurements of the linewidth is 10 km s^{-1} and that on *H*-band magnitudes is 0.15 mag. The TF relation for the 73 galaxies used in the derivation of the template is shown in Fig. 2(c). The best-fitting template, obtained using the bivariate method (Giovanelli et al. 1997) is given by: $H = -2.60 - 7.85 \log W_c$. The scatter of the TF template, thus the uncertainty in the distance modulus of the individual galaxies, is 0.35 mag.

The zero-point and slope of the TF template relation are found to be consistent with the parameters of the local TF calibrators.

The TF relation of Virgo late-type galaxies is given in Fig. 2(b), with the template relation superposed. The scatter of Virgo galaxies is 0.70 mag, thus significantly larger than that of the template relation. We have checked whether the threshold of the galaxy inclination adopted by us is insufficiently conservative and may have produced this large scatter. However, we found that for galaxies with inclination $i > 45°$ the scatter remains 0.70 mag. Also, we determined that the scatter is not affected by the inclusion of galaxies with H I deficiency larger than 0.7. In Figs 2(a) and (c) all Virgo cluster galaxies are assumed to have a distance modulus equal to the average distance modulus of Virgo cluster A ($\mu_0 = 31.02$). Templates shifted by ± 1 mag are also given. The deviations of the individual objects from the template relations can be converted into distances to the individual galaxies.

5 RESULTS

5.1 Derived distances

The distances to 134 galaxies in the Virgo cluster are listed in Tables 2 and 3.

Table 2 lists the TF parameters of 75 late-type galaxies as follows:

Columns 1–3: CGCG, NGC, VCC designations.

Column 4: Morphological type as given in the VCC.

Column 5: Membership according to the VCC (revised by Binggeli et al. 1993).

Column 6: H I deficiency parameter as defined by Haynes & Giovanelli (1984).

Column 7: Total *H*-band magnitude corrected for internal extinction (see Section 3.1).

Column 8: NIR observing run: CA96 refers to Boselli et al. (1997), CA97 are the observations taken in 1997 at Calar Alto (see Section 3.1), and T95 and T96 are TIRGO runs found in Gavazzi et al. (1996a).

Column 9: Heliocentric recessional velocity from the literature.

Column 10: Adopted logarithm of the maximum rotational velocity, corrected for inclination, as derived from H I observations (average of 20 per cent and 50 per cent of the peak value) or from CO observations or Hα rotation curves (see Table 1).

Column 11: A quality mark given to each H I profile after individual inspection: 1 are two-horn, high S/N profiles; 2 are one-horn, high S/N profiles; 5 is for one profile that was not published, but was considered of good quality given the high S/N ratio.

Column 12: Galaxy inclination in the plane of the sky (determined following Haynes & Giovanelli 1984).

Column 13: Reference to the adopted rotational velocity.

Column 14: Distance modulus as obtained in this work using the TF method.

Column 15: Revised region of membership (see Section 5.3 for definition).

A comment is given in column 16 for the deficient galaxies whose maximum rotational velocity is derived from CO profiles or Hα rotation curves (see Table 1).

Table 3 lists the FP parameters of 59 early-type galaxies as follows:

Columns 1–5: Contain the same information as Table 2.

Column 6: Heliocentric recessional velocity.

Columns 7–9: Central velocity dispersion with error (given for the OHP measurements only) and reference. McElroy (1995, M95) did a compilation of all dispersion measurements available at the time. Not only are the values averages of various sources, but they are also corrected for aperture according to the prescriptions of Jørgensen et al. (1996). Our data (this work, T.W.) are taken through a 2×6 arcsec^2 aperture, corrected similarly (see Section 3.4).

Columns 10–11: Logarithm of the *H*-band effective radius r_e, corrected for seeing according to the prescriptions of Saglia et al. (1993), with uncertainty (in arcsec).

Columns 12–13: Corrected *H*-band effective surface brightness with uncertainty (in mag arcsec^{-2}). The correction includes the cosmological expansion $(1+z)^4$ and *k*-correction (taken to be proportional to $1+z$) terms, and the seeing correction, according to Saglia et al. (1993). No galactic absorption correction was applied since $A_H = 0.085 A_B$ (Pahre, Djorgovski & de Carvalho 1995), with $A_B \leq 0.1$ mag in the direction of Virgo.

Column 14: Seeing during the *H*-band observations.

Column 15: NIR observing run: T97 refers to the 1997 run at TIRGO (this work); nine objects were serendipitously observed at Calar Alto (C94–96) in K' band and are found in Boselli et al. (1997); one of the T97 objects was also serendipitously observed at Calar Alto in 1997 in *H* band.

Column 16: Distance modulus as obtained in this work using the FP method.

Column 17: Revised region of membership (see Section 5.3 for definition).

5.2 Comparison with independent distance estimates

Because many different methods have been applied to derive distance estimates to Virgo galaxies, a number of consistency checks can be made between our TF and FP distance determinations and those obtained independently by other groups, either with the same or with different methods. Fig. 3(a) shows the comparison of our own distance estimates with those in the literature, obtained with methods other than the TF or FP relation: Cepheids, Type I and II supernovae, planetary nebulae luminosity function, novae, globular clusters luminosity function, and surface brightness fluctuations. The rms scatter in the distance modulus differences, when measured for E/S0 galaxies alone, is larger (0.40 mag) than that measured for the spiral galaxies (0.33 mag), even if we exclude objects with $\sigma < 100$ km s^{-1}. This latter comparison is based on distance estimates obtained using Cepheids and Type I and II supernovae methods. Assuming that these methods have an average

Table 2. Derived parameters of late-type galaxies.

CGCG (1)	NGC (2)	VCC (3)	T (4)	Memb (5)	Def_{H_I} (6)	H_c (7)	Ref[a] (8)	V_{hel} (9)	log W_c (10)	Qual (11)	i (12)	Ref[b] (13)	μ_0 (14)	Region (15)	Comments (16)
98077	4152	25	Sc	M	−0.28	9.84	CA97	2168	2.60	1	35.8	HH84	32.85	M	
69083	I769	58	Sb	M	0.05	10.38	CA97	2207	2.54	1	47.2	HH84	32.92	M	
69088	4178	66	Sc	m	−0.17	8.95	CA96	369	2.46	1	67.3	W86	30.86	N	
41048	4180	73	Sb	W	0.20	9.31	CA97	2082	2.65	2	68.1	HL89	32.72	W	
98108	4192	92	Sb	A	0.13	6.72	CA96	−132	2.68	1	73.4	CG90	30.36	N	
69091	4193	97	Sc	M	0.14	9.55	CA97	2466	2.61	1	58.0	HH84	32.64	M	
41052	4197	120	Sc	m	0.21	10.08	CA97	2064	2.45	1	81.0	HH84	31.91	W	
69104	4206	145	Sc	m	0.30	9.38	CA97	702	2.46	1	77.8	HH84	31.29	N	
69107	4207	152	Sc	m	0.01	9.64	CA96	596	2.40	1	57.1	HL89	31.08	N	
69110	4212	157	Sc	A	0.48	8.26	CA97	−83	2.57	1	46.5	HH84	31.04	N	
69112	4216	167	Sb	A	0.46	6.54	CA97	140	2.74	1	78.5	CG90	30.65	N	
98130	4237	226	Sc	A	0.46	8.86	CA97	863	2.55	1	46.5	HH84	31.48	N	
41069	I3115	267	Sbc	p	−0.03	11.19	CA97	733	2.33	1	36.0	HL89	32.08	B	
42008	–	324	Irr	W	−0.17	12.17	CA97	1524	2.06	2	31.2	HH87	30.94	S	
42028	4273	382	Sc	W	−0.11	9.26	CA97	2378	2.59	1	47.8	HH84	32.19	W	
99023	4293	460	Sa	A	0.56	7.44	CA96	948	2.61	5	66.0	B90	30.53	A	
70024	4294	465	Sc	A	−0.08	9.65	CA97	357	2.37	1	65.4	HH84	30.86	N	
99027	4302	497	Sc	A	0.29	7.92	CA97	1150	2.58	1	78.8	HH84	30.78	A	
70029	4307	524	Sbc	B	1.35	9.67	T95	1092	2.52	–	77.8	T.W.	32.05	B	see Table 1
99029	4312	559	Sab	A	1.24	8.79	CA97	153	2.35	1	78.3	HH84	29.84	A	see Table 1
70034	4313	570	Sab	A	1.09	8.58	CA97	1443	2.44	1	77.7	HH84	30.34	A	see Table 1
70035	4316	576	Sbc	B	0.17	9.32	CA97	1254	2.52	1	81.4	HG86	31.70	B	
99030	4321	596	Sc	A	0.29	6.79	CA97	1575	2.73	1	27.1	HG81	30.82	A	$i < 30$, Ceph.
42063	4324	613	Sa	W	−0.07	8.57	CA97	1670	2.55	1	64.4	HW89	31.19	S	
70039	4330	630	Irr	A	0.90	9.55	CA97	1564	2.44	1	76.6	HH84	31.31	A	see Table 1
42070	4343	656	Sb	W'	0.46	9.09	CA97	1014	2.55	1	75.0	HH84	31.71	B	
70045	4351	692	Sc	A	0.38	10.45	CA96	2324	2.22	1	45.2	HG81	30.48	A	
42093	4376	787	Sc	m	0.18	11.08	CA97	1136	2.32	1	54.3	S90	31.89	B	
70061	4380	792	Sab	B	0.89	8.48	CA97	971	2.63	–	54.5	T.W.	31.73	B	see Table 1
99044	4383	801	Irr	A	−0.69	9.59	CA97	1710	2.42	1	57.1	HH84	31.19	A	
42095	I3322	827	Sc	B	0.11	9.51	CA97	992	2.48	1	83.3	HG86	31.58	B	
70068	4388	836	Sab	A	0.83	8.12	CA96	2515	2.60	1	78.8	HG81	31.13	A	see Table 1
70067	4390	849	Sbc	A	0.21	10.73	CA97	1103	2.39	1	37.8	SA82	32.09	B	
99049	4396	865	Sc	A	0.45	10.26	CA97	−124	2.31	1	71.1	S90	31.00	A	
70071	4402	873	Sc	A	0.63	8.46	CA96	234	2.45	1	72.0	HH84	30.29	A	
70076	4413	912	Sbc	A	0.76	9.72	CA96	105	2.38	–	48.1	B95	31.01	A	see Table 1
42106	4420	957	Sc	W	−0.13	9.72	CA97	1688	2.37	1	58.8	HR86	30.93	S	
99054	4419	958	Sa	A	1.05	7.80	CA97	−273	2.62	–	72.5	S95-KY88	30.97	A	see Table 1
42107	4423	971	Sc	m	−0.05	11.36	CA96	1120	2.24	2	84.4	HW84	31.55	B	
70097	4438	1043	Sb	A	1.25	7.17	CA96	70	2.67	–	67.4	CS85-K95	30.26	A	see Table 1
70104	4445	1086	S	B	1.26	9.74	CA97	167	2.41	–	90.0	T.W.	31.26	A	see Table 1
99062	4450	1110	Sab	A	0.87	7.03	CA96	1954	2.66	1	44.7	HH84	30.51	A	see Table 1
70111	4451	1118	Sc	B	0.44	10.01	CA97	862	2.49	1	45.2	GK83	32.16	B	
99065	I3392	1126	Sb	A	1.05	9.31	CA97	1687	2.35	1	63.9	HL89	30.36	A	see Table 1
42124	4457	1145	Sb	S	0.83	7.92	CA97	884	2.50	–	34.3	T89	30.15	S	see Table 1
70121	4469	1190	Sa	B	>1.76	8.19	CA97	508	2.59	–	71.9	T.W.	31.12	A	see Table 1
42132	4470	1205	Sc	p	−0.16	10.21	CA97	2339	2.35	1	40.9	HH84	31.26	S	
42139	4480	1290	Sb	W	−0.02	9.78	T96	2438	2.58	1	58.1	HH84	32.64	S	
99075	4498	1379	Sc	A	0.35	9.78	CA96	1505	2.37	1	58.0	HH84	30.99	A	
99077	I797	1393	Sc	p	0.03	11.02	CA97	2091	2.32	1	46.5	HR86	31.83	A	
99076	4501	1401	Sbc	A	0.43	6.29	CA97	2284	2.80	1	56.6	HH84	30.87	A	
70167	4519	1508	Sc	B	−0.18	9.65	CA97	1212	2.43	1	43.9	HH84	31.33	S	
70168	4522	1516	Sbc	B	0.76	9.74	CA97	2330	2.34	–	73.8	T.W.	30.71	S	see Table 1
99090	I800	1532	Sc	p	0.72	10.82	CA97	2335	2.23	2	40.9	HG86	30.93	A	see Table 1
42156	4527	1540	Sb	W	−0.23	7.02	CA97	1736	2.60	1	71.1	HW89	30.03	S	
42158	4532	1554	Irr	B	−0.16	9.49	CA96	2021	2.31	1	64.7	HH84	30.23	S	
42159	4535	1555	Sc	B	0.13	6.97	CA97	1962	2.62	1	42.4	HH84	30.67	S	
14068	4536	1562	Sc	W	0.07	7.64	CA97	1807	2.60	1	62.7	P79	30.65	S	
42162	I3521	1575	Irr	B	0.47	11.04	CA96	597	2.24	2	40.9	HL89	31.23	S	
99093	4540	1588	Sc	A	0.51	9.46	CA97	1288	2.35	1	35.8	S90	30.51	A	
99096	4548	1615	Sb	A	0.63	7.40	CA96	483	2.66	1	36.3	CG90	30.88	A	
42168	4544	1624	Sc	S	0.67	10.20	CA97	1151	2.34	1	68.4	HW89	31.17	S	
70191	I3583	1686	Sm	A	0.65	11.36	CA96	1121	2.13	1	52.3	HH87	30.68	A	

Table 2 – *continued*

CGCG (1)	NGC (2)	VCC (3)	T (4)	Memb (5)	$Def_{H\,I}$ (6)	H_c (7)	Ref[a] (8)	V_{hel} (9)	log W_c (10)	Qual (11)	i (12)	Ref[b] (13)	μ_0 (14)	Region (15)	Comments (16)
70192	4569	1690	Sab	A	1.20	6.73	CA96	−212	2.68	–	62.8	CS85	30.37	A	see Table 1
70194	4571	1696	Sc	A	0.55	8.71	CA97	342	2.56	1	27.1	HH84	31.41	A	$i < 30$, Ceph.
70197	4579	1727	Sab	A	0.81	6.71	CA96	1512	2.84	1	36.5	CG90	31.61	A	see Table 1
42187	4586	1760	Sa	S	1.08	8.64	CA97	792	2.44	1	72.5	HH84	30.40	S	see Table 1
99106	4595	1811	Sc	A	0.11	10.20	CA96	632	2.31	1	47.8	HH84	30.94	E	
42208	4630	1923	Sbc	S	0.17	9.94	T96	742	2.34	1	42.7	HL89	30.91	S	
99111	4633	1929	Sc	A	0.51	10.67	CA96	291	2.32	1	64.7	S90	31.48	E	
70230	4639	1943	Sb	A	0.10	8.83	CA97	1048	2.62	1	44.4	HG81	32.00	E	
71015	4647	1972	Sc	A	0.41	8.65	CA96	1422	2.54	1	35.8	HH84	31.19	E	
71019	4654	1987	Sc	A	−0.23	7.74	CA96	1039	2.60	1	51.4	HG81	30.75	E	
71032	I3742	2023	Sc	A	0.58	11.52	CA96	967	2.31	1	60.4	HG86	32.25	E	
71045	4698	2070	Sa	m	−0.33	7.65	CA96	1008	2.71	1	57.2	HH84	31.53	E	

[a] CA96: Calar Alto observations from Boselli et al. (1997); CA97: Calar Alto observations taken in 1997 (see Section 3.1); T95, T96: TIRGO observations in Gavazzi et al. (1996a).
[b] B90: Bottinelli et al. 1990; B95: Boselli et al. 1995; CG90: Cayatte et al. 1990; CS85: Chincarini & de Souza 1985; GK83: Giovanardi, Krumm & Salpeter 1983; H96: Hoffman et al. 1996; HG81: Helou et al. 1981; HG86: Haynes & Giovanelli 1986; HH84: Helou, Hoffman & Salpeter 1984; HH87: Hoffman et al. 1987; HL89: Hoffman et al. 1989a; HR86: Hutchtmeier & Richter 1936; HW89: Hoffman et al. 1989b; K95: Kenney et al. 1995; KY88: Kenney & Young 1988; P79: Peterson 1979; S90: Schneider et al. 1990; S95: Speraindio et al. 1995; SA82: Sulentic & Arp 1982; T89: Thronson et al. 1989; T.W.: this work; W86: Warmels 1986.

intrinsic accuracy of 0.2 mag, this implies that our TF uncertainty is ∼0.25 mag.

The comparison for E/S0 galaxies is based on distance estimates obtained using the following methods: surface brightness fluctuation (Tonry et al. 1990; Jensen et al. 1996; Ajhar et al. 1997; Morris & Shanks 1998), novae luminosities (Della Valle & Livio 1995), the globular clusters luminosity function (Secker & Harris 1993; Whitmore et al. 1995; van den Bergh 1996), and the planetary nebulae luminosity function (Jacoby et al. 1990; Ciardullo et al. 1998). Assuming once again that these methods have an average intrinsic accuracy of 0.2 mag, this implies that our FP accuracy is ∼0.35 mag.

Fig. 3(b) compares our TF distances with the recent *B*-band TF compilation of Yasuda et al. (1997). The rms scatter is 0.47 mag, which would correspond to an accuracy of each separate measurement (assuming equal contributions to the scatter) of roughly 0.3 mag. This is in good agreement with the internal accuracy estimate of Yasuda et al. (1997), but it is surprisingly larger than the accuracy estimate derived above from the comparison with non-TF-based distance estimates of S galaxies, which should be contributed to by both measurement uncertainties and intrinsic variations in galaxy properties.

Unfortunately a similar comparison cannot be made with the Federspiel et al. (1998) distances, which were not published individually.

Distances obtained in this work with the FP method ($\sigma > 100$ km s^{-1}) are compared in Fig. 3(c) with those obtained in the *B* band by Dressler et al. (1987) and Dressler (1987) with the Dn-σ method. The agreement is not very satisfactory, with a systematic offset of 0.10 mag and an rms scatter of 0.40 mag. Since the accuracy of the *B*-band Dn-σ method is expected to be slightly worse than that of the FP method, we conclude that the observational scatter of our FP distance determination is at most 0.3 mag.

A test for the internal consistency between our TF and FP distance determinations can be done using the interacting system NGC 4435 (S0) + NGC 4438 (S). The distance moduli of the two galaxies (30.59 and 30.26 respectively) agree within the errors. Similarly, the pair NGC 4649 (S0) + NGC 4647 (S) has consistent distance moduli (31.37 and 31.19 respectively). A test of the reproducibility of our results can be done with the galaxy NGC 4261, which was observed both at TIRGO in 1997 and, serendipitously, at Calar Alto in 1997; the difference between the distance moduli based on the two separate observations is 0.15 mag.

A discrepancy is found between our FP-based determination of the distance of M87, and other determinations found in the literature. Our value $\mu_0 = 31.62$ is larger than 31.30 (van den Bergh 1996), 31.12 (Whitmore et al. 1995) and 30.79 (Ciardullo et al. 1998). The discrepancy most likely arises from an underestimate of the total *H* magnitude of M87 on our part, owing to the fact that M87 fills the TIRGO frame (approximately 4 arcmin), thus affecting the estimate of the sky background. Conversely the distance of M49 found in this work, $\mu_0 = 31.18$, is in excellent agreement with Tonry et al. (1990) ($\mu_0 = 31.18$) and consistent with the most recent determination by Morris & Shanks (1998) ($\mu_0 = 30.97$).

5.3 The 3D structure of the Virgo cluster

The newly obtained distance moduli are plotted against V_{LG} in Fig. 4, where small dots mark the early-type galaxies (FP), separated into $\sigma < 100$ km s^{-1} and $\sigma > 100$ km s^{-1}, and larger circles mark the spirals (TF), separated into normal and H I deficient. The dashed line represents the Hubble flow, drawn for $H_0 = 81.35$. Distance moduli derived with the TF and FP relation have similar distributions and mean values. H I-deficient objects have TF distances not different from galaxies with normal H I content. Conversely the FP distances of galaxies with $\sigma < 100$ km s^{-1} are significantly smaller and with higher rms uncertainty than those with larger dispersion. Notice that the four galaxies with the smallest distance estimates are among the objects with the smallest velocity dispersions ($\sigma \sim 50-80$ km s^{-1}). Accordingly their distance estimate uncertainties must be quite large, up to the point that we cannot trust them. As anticipated in Section 4.1, these galaxies are thus excluded from the rest of the analysis.

Three arbitrary regions are evidenced in the figure: $\mu_0 < 31.5$ and $\mu_0 > 31.5$. The latter is split in two velocity regions: above and below 1900 km s^{-1}. The region delimited by $30 < \mu_0 < 31.5$

Table 3. Derived parameters of early-type galaxies.

CGCG (1)	NGC (2)	VCC (3)	T (4)	Memb (5)	V_{hel} (6)	σ (7)	$\pm$ (8)	Ref[a] (9)	log r_{eH} (10)	$\pm$ (11)	μ_e (12)	$\pm$ (13)	Seeing (14)	Ref[b] (15)	μ_0 (16)	Region (17)
69081	4168	49	E	M	2307	186	–	M95	1.61	0.01	17.92	0.03	1.9	T97	32.67	M
69096	4200	122	S0	M	2376	80	–	M95	1.46	0.05	18.72	0.13	2.5	T97	31.92	M
41055	4215	166	S0	W	2073	152	7	T.W.	1.44	0.03	17.25	0.07	3.0	T97	31.78	W
41063	4233	220	S0	W	2224	205	5	T.W.	1.00	0.02	15.78	0.07	2.6	T97	32.59	W
42004	4255	312	S0	W	1696	172	11	T.W.	0.64	0.05	14.83	0.18	3.5	T97	32.29	W
42012	4259	342	S0	W	2401	151	–	M95	1.37	0.05	18.29	0.12	2.3	T97	33.78	W
42013	4261	345	E	W	2200	326	–	M95	1.45	0.01	16.44	0.04	2.7	T97,C97	32.79	W
99014	4262	355	S0	A	1369	188	–	M95	0.72	0.02	13.98	0.06	2.4	T97	30.86	A
70013	4267	369	S0	A	1009	160	–	M95	0.96	0.01	15.05	0.04	2.1	T97	30.83	N
42026	4270	375	S0	W	2347	138	11	T.W.	–	–	–	–	–	–	–	–
42040	4292	462	S0a	W	2258	53	–	M95	2.00	0.05	19.99	0.07	1.9	T97	29.88	S
42059	4318	575	E	B	1229	100	–	M95	1.31	0.04	17.85	0.10	2.9	T97	32.02	B
99036	4340	654	S0	A	930	113	–	M95	1.25	0.01	16.66	0.04	1.9	T97	30.83	A
99038	4350	685	S0	A	1241	189	–	M95	1.36	0.02	15.97	0.06	2.1	T97	30.86	A
70057	4371	759	S0	A	943	125	–	M95	1.77	0.02	17.70	0.04	2.3	T97	30.20	A
70058	4374	763	E	A	910	296	–	M95	1.53	0.01	15.90	0.02	2.3	T97	31.36	A
99041	4377	778	S0	A	1371	141	–	M95	0.82	0.02	14.96	0.07	1.8	T97	30.95	A
99042	4379	784	S0	A	1069	70	–	M95	1.35	0.03	17.06	0.07	2.1	T97	29.39	A
70065	4387	828	E	A	583	112	–	M95	1.67	0.01	18.12	0.03	1.9	T97	31.00	A
70080	4417	944	S0	B	832	84	–	M95	1.56	0.01	16.97	0.02	1.5	T97	28.76	A
99055	4421	966	S0	A	1603	90	6	T.W.	1.62	0.03	18.23	0.08	2.0	T97	30.70	A
70093	4429	1003	S0	A	1130	182	–	M95	2.01	0.03	17.90	0.07	3.8	C96	30.57	A
70094	4431	1010	S0	A	913	68	–	M95	2.59	0.05	21.67	0.08	2.4	T97	30.45	A
42115	4434	1025	E	B	1068	115	–	M95	1.04	0.01	16.26	0.04	1.6	T97	31.28	S
70098	4435	1030	S0	A	775	168	–	M95	1.37	0.01	16.09	0.04	2.3	C96	30.59	A
70099	4440	1047	Sa	A	724	110	7	T.W.	1.25	0.02	16.96	0.05	1.7	C94	31.19	A
70100	4442	1062	S0	B	517	171	8	T.W.	–	–	–	–	–	–	–	–
70114	4458	1146	E	A	662	106	–	M95	1.26	0.02	17.55	0.07	1.7	T97	31.99	A
70116	4459	1154	S0	A	1210	178	–	M95	1.43	0.01	16.23	0.02	1.8	T97	30.72	A
70115	4461	1158	Sa	A	1919	118	7	T.W.	1.66	0.01	17.60	0.02	2.6	C94	30.40	A
42128	4464	1178	E	B	1199	121	–	M95	0.96	0.02	15.94	0.06	2.7	T97	31.32	S
42134	4472	1226	E	B	997	303	–	M95	1.70	0.04	16.26	0.10	2.0	–	31.18	S M49
70125	4473	1231	E	A	2236	193	–	M95	1.34	0.01	15.47	0.02	1.7	T97	30.19	A
70127	4474	1242	S0	A	1610	117	9	T.W.	1.44	0.02	17.25	0.05	2.0	T97	30.90	A
70129	4477	1253	S0	A	1353	177	–	M95	1.55	0.01	16.84	0.03	2.9	C96	31.08	A
70133	4478	1279	E	A	1370	143	–	M95	1.76	0.03	17.77	0.07	2.2	T97	30.82	A
70136	4483	1303	S0	B	875	106	4	T.W.	1.48	0.02	17.97	0.06	2.0	T97	31.53	B
70139	4486	1316	E	A	1292	333	–	M95	1.99	0.01	17.26	0.02	1.8	T97	31.62	A M87
70137	4488	1318	S0	B	980	54	4	T.W.	2.16	0.03	20.22	0.06	2.0	T97	29.53	A
99073	4489	1321	S0	A	930	62	–	M95	1.14	0.02	17.18	0.05	1.6	T97	30.22	A
70149	4503	1412	Sa	A	1342	120	7	T.W.	1.76	0.01	17.86	0.02	1.3	C94	30.35	A
99086	4515	1475	E	A	940	91	–	M95	0.91	0.02	16.06	0.06	1.5	T97	30.82	A
42155	4526	1535	S0	B	533	267	–	M95	1.74	0.01	16.48	0.03	2.6	T97	30.91	S
70172	4528	1537	S0	A	1374	107	–	M95	1.43	0.02	17.33	0.06	1.8	T97	30.81	A
70183	4551	1630	E	A	1198	113	–	M95	1.65	0.02	18.10	0.04	1.8	T97	31.13	A
70184	4552	1632	S0	A	322	269	–	M95	1.31	0.01	15.47	0.03	1.7	T97	31.46	A
70186	4564	1664	E	A	1165	160	–	M95	1.54	0.02	16.79	0.04	1.9	T97	30.72	A
42178	4570	1692	S0	B	1730	186	–	M95	1.51	0.01	16.38	0.03	2.1	T97	30.70	S
70195	4578	1720	S0	A	2284	127	–	M95	1.32	0.02	16.96	0.06	1.9	T97	31.32	E
70207	4598	1827	S0	A	1961	92	–	M95	2.20	0.03	20.92	0.05	1.6	T97	32.17	E
70214	4608	1869	S0	A	1864	157	–	M95	1.63	0.01	17.62	0.02	2.1	C96	31.53	E
42205	4612	1883	S0	m	1875	104	5	T.W.	1.22	0.01	16.71	0.04	1.8	T97	30.74	S
70223	4621	1903	E	A	444	230	–	M95	1.56	0.01	16.26	0.02	1.8	T97	30.95	E
42207	4623	1913	E	m	1892	89	–	M95	1.98	0.02	19.33	0.04	1.6	T97	30.63	E
70229	4638	1938	S0	A	1147	132	–	M95	1.63	0.03	16.86	0.06	1.6	T97	29.74	E
43002	4636	1939	E	S	937	207	–	M95	1.72	0.01	17.19	0.03	1.9	T97	31.29	S
71016	4649	1978	S0	A	1095	339	–	M95	1.84	0.01	16.58	0.01	2.3	C96	31.37	E
71023	4660	2000	E	A	1115	185	–	M95	1.14	0.01	15.32	0.04	1.6	T97	30.83	E
71054	4733	2087	S0	A	905	75	–	M95	1.98	0.02	19.70	0.04	2.1	C96	30.67	E
71062	4754	2092	S0	A	1377	200	–	M95	1.42	0.01	16.32	0.03	2.0	T97	31.29	E
71065	4762	2095	S0	A	984	147	–	M95	1.86	0.04	17.62	0.08	2.6	T97	30.17	E

[a] M95, McElroy (1995); T.W., this work.
[b] C94–96, serendipitously observed in K' band at Calar Alto (see Boselli et al. 1997).

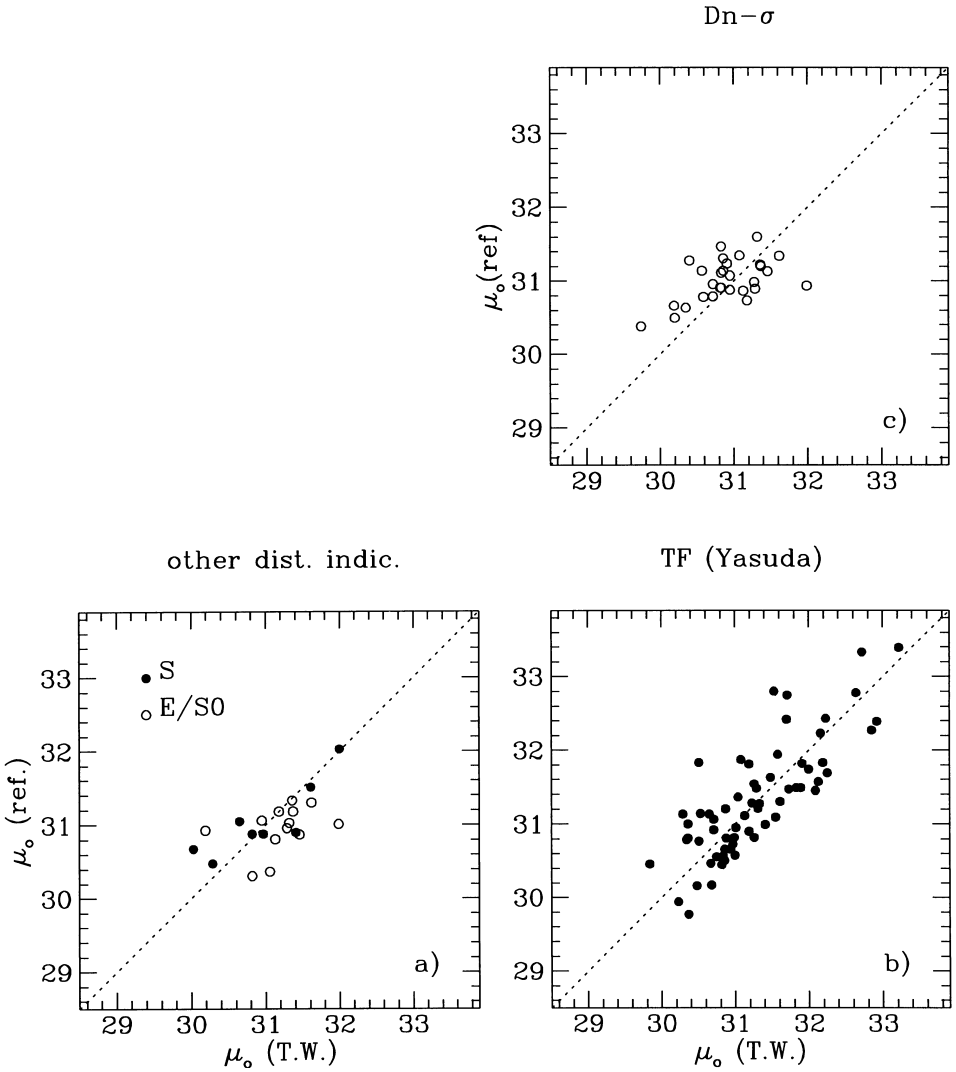

Figure 3. (a) The comparison between the distance moduli obtained in this work with those available in the literature, obtained with other than Tully–Fisher methods. (b) The comparison between the distance moduli obtained in this work with the *H*-band TF method, with the *B*-band ones obtained by Yasuda et al. (1997). (c) The comparison between the distance moduli obtained in this work (for $\sigma > 100$ km s^{-1}) and those obtained with the Dn-σ method in the *B* band. The dotted line is drawn to indicate the one-to-one relationship.

contains the majority of galaxies at the distance to the Virgo cluster. This region contains the majority of H I-deficient galaxies.

A better insight into the structure of the cluster is obtained with Fig. 5, which reports the same data as Fig. 4, but with symbols whose size decreases with increasing distance, and whose shape refers to seven regions of the Virgo cluster, represented in Fig. 6 with dotted lines (galaxies with $\sigma < 100$ km s^{-1} are omitted). Galaxies are assigned to these regions with a criterion that combines their position on the sky with their distance and redshift.

Distant ($\mu_0 > 31.5$) galaxies with $V_{\rm LG} > 1900$ belong almost exclusively to the regions marked M and W. These correspond to the M and W clouds, which thus are found to be in Hubble flow.

Distant ($\mu_0 > 31.5$) objects with $V_{\rm LG} < 1900$ mostly belong to the region marked B. This corresponds to cluster B of Binggeli et al. (1993), but with a smaller extent than in the original definition. The mean distance modulus for this structure is found to be 31.84, in good agreement with the determination by Federspiel et al. (1998) ($\mu_0 = 31.8$). To the east of approximately $\alpha = 12^{\rm h}25^{\rm m}$ (M49) all galaxies have distances not dissimilar from those of cluster A ($\mu_0 \sim 31$). For example four spiral galaxies (NGC 4519, 4332 and 4535, and IC 3521), which are assigned to cluster B by Binggeli et al. (1985), are not confirmed to lie at significantly larger distance than cluster A, since they are found at $\mu_0 = 30.2$–31.3. For these objects our TF distance determinations are in agreement with those of Yasuda et al. (1997). Another three E/S0 cluster B candidates according to Binggeli et al. (NGC 4472 (M49), 4526 and 4570) have $\mu_0 < 31.2$, as determined using the FP relation. Our low distance estimate of M49 agrees with independent estimates obtained using all methods quoted above. Unfortunately this is the only galaxy with independent distance estimate among this group of early-type objects. We propose that M49 belongs to cloud S. Its redshift ($V_{\rm LG} = 1200$ km s^{-1}) is 400 km s^{-1} lower than the mean, but it is well within the distribution of $V_{\rm LG}$ in this region.

The remaining galaxies have $\mu_0 < 31.5$. They form the main body of the cluster, indicated here with region A (M87), N to the north-west, E to the east, and S to the south.

Region A coincides with cluster A and with the X-ray position (see Fig. 7 adapted from Böhringer et al. 1994, reproduced on the same scale as Fig. 6). As expected, most H I-deficient galaxies belong to this region (see Fig. 8). Two exceptions are surprisingly

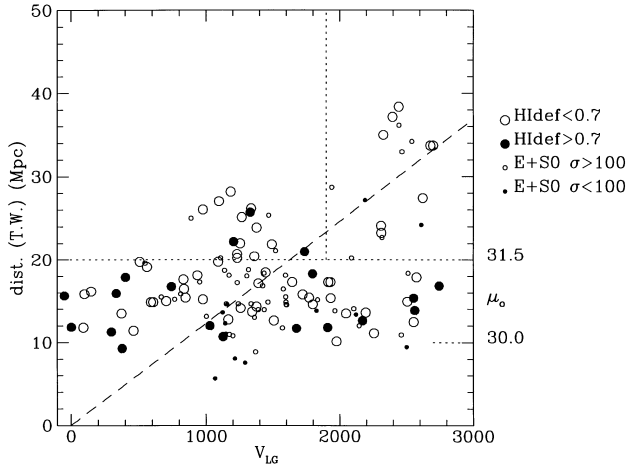

Figure 4. The distances obtained in this work plotted against $V_{\rm LG}$. Small dots mark the early-type galaxies (FP), separated into $\sigma < 100$ and $\sigma > 100$ km s^{-1}. Larger circles mark the spirals (TF), separated into normal and H I-deficient. The broken line represents the Hubble flow, for $H_0 = 81.35$ km s^{-1} Mpc^{-1}.

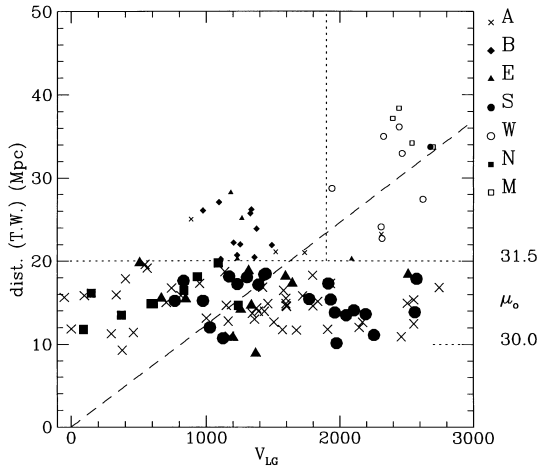

Figure 5. Same as Fig. 4 with symbol size decreasing with increasing distance and whose shape refers to seven regions of the Virgo cluster, represented in Fig. 6 with dotted lines.

found at the southern edge of the cluster in the region of NGC 4636, a strong and extended X-ray source (Trinchieri et al. 1994). We argue that a significant quantity of extended gas must be associated with this galaxy.

The distribution of μ_0 in the cluster A itself is centred at $\mu_0 = 30.84$[2] with a dispersion of 0.45 mag. This is comparable to the nominal uncertainty of the distance determination methods (0.35 and 0.45 mag for TF and FP), and thus the depth along the line of sight of this aggregate cannot be determined.

One of the most interesting results of the present analysis is that, among galaxies at the main cluster distance, those belonging to clouds N and S show a significant velocity segregation. This is illustrated in Fig. 9. The two rightmost panels of this figure give histograms of $V_{\rm LG}$ and of μ_0 derived from this work for the seven considered regions. While the distances of cluster A and clouds S, N and E are in agreement ($\mu_0 = 30.84$–31.23), the only significantly more distant structures are cluster B and clouds W and M. Clusters A and B and cloud E have similar velocity distributions peaked at the standard $V_{\rm LG} \sim 1350$ km s^{-1}. Clouds W and M have instead a higher velocity. Clouds S and N have significantly different distributions. The N one contains galaxies with $V_{\rm LG} < 1300$ km s^{-1}, thus blueshifted with respect to Virgo. Similar evidence was pointed out by Hoffmann et al. (1989b) and was extensively analysed by Tully & Shaya (1984) to model the infall of galaxies on the Virgo cluster. On the contrary, cloud S contains mainly redshifted galaxies, with $750 < V_{\rm LG} < 2700$ km s^{-1}. To check if the latter result is not caused by the limited statistics of the sample used in this work, and since the velocity distribution can be derived from a larger body of velocity measurements than the one represented in our sample of galaxies with distance estimates, we determine the velocity distributions in the seven studied regions using the whole VCC (which contains over 400 galaxies with redshift estimates) (see left panel of Fig. 9). The difference between regions S and N, noticed in our smaller sample with distance estimates, is equally

[2] It is important to stress once more that the absolute distance of cluster A is not an independent result of this work, since a distance of Virgo = 16 Mpc has been assumed to calibrate the zero-point of both the TF and FP template relations.

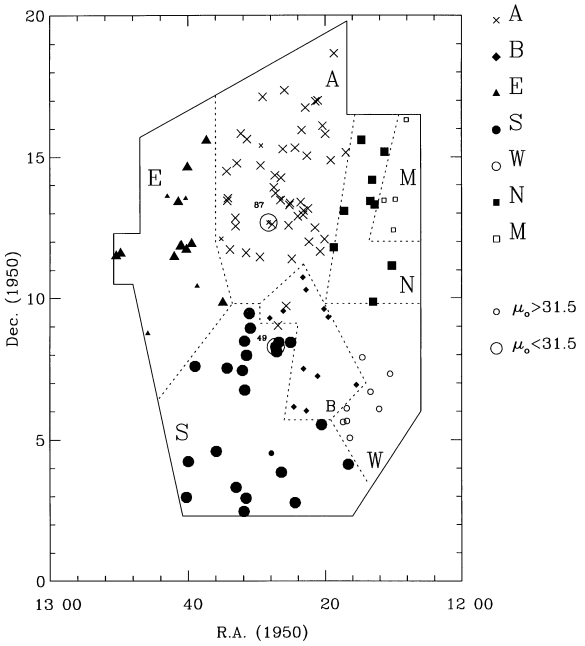

Figure 6. The distribution in celestial coordinates of 134 galaxies with distance estimates obtained in this work in the region covered by the VCC (solid line). The seven regions of revised membership are given con toured by broken lines. Symbol sizes decrease with increasing distance (as in Fig. 5). The positions of M49 and M87 are marked.

present in the larger VCC sample, and we conclude that it represents a real difference between the two clouds.

A summary of the mean velocity, velocity dispersion, and distance modulus determinations for all seven regions is presented in Table 4, and is also shown in Fig. 10, where the average velocities and distance moduli are plotted with error bars indicating the statistical uncertainties on the determination of the two quantities (galaxies with $\sigma < 100$ km s^{-1} are excluded). Estimates of cluster A are also given separately for early-type and late-type galaxies, subdivided into H I deficient and H I normal. Mean quantities and the associated uncertainties were computed using the so-called

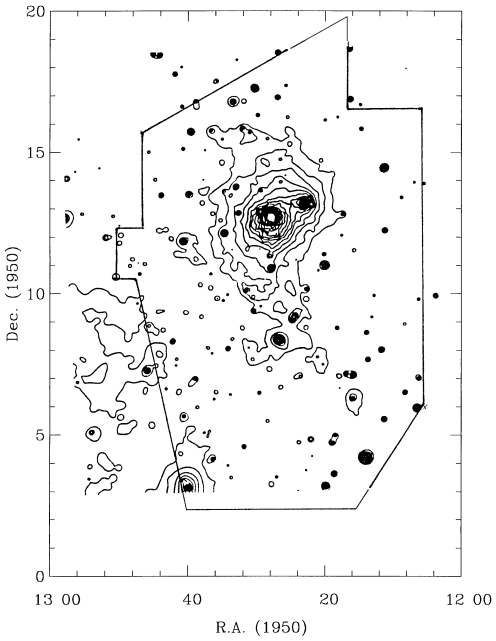

Figure 7. The *ROSAT* all-sky map of Virgo, adapted from Böhringer et al. (1994) on the same scale as Fig. 6. Reprinted with permission from *Nature* (Vol. 368, p. 828). Copyright (1994) Macmillan Magazines Limited.

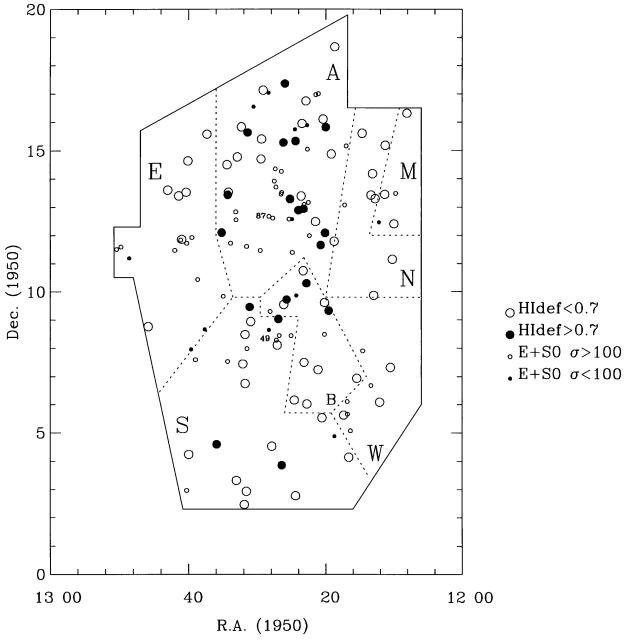

Figure 8. The distribution in celestial coordinates of 134 galaxies with distance estimates. Small dots mark the early-type galaxies (FP) (for $\sigma > 100$ km s^{-1}) and larger circles mark the spirals (TF), separated into normal and H I-deficient (as in Fig. 4). The positions of M49 and M87 are marked.

biweight estimators (see Beers, Flynn & Gebhardt 1990 for details), which are known to provide a robust parameter estimation for samples covering a wide interval in size. Statistical uncertainties on the distance modulus determinations are obtained by adding in quadrature the uncertainty on the FP template zero-point determination and the uncertainty with which a given sample distance is determined (taking into account the dispersion that characterizes the FP relation). These should be conservative estimates, since the uncertainties associated with the TF relation, which is used to derive 60 per cent of the distance estimates, are somewhat smaller than those associated with the FP. The last two columns of Table 4 list the peculiar velocities of the Virgo clouds with respect to cluster A [computed as the difference between the actual velocity of the various entities (column 3) and their Hubble flow velocity, minus 156 km s^{-1}, which represents the deviation of cluster A itself from the Hubble flow] with statistical uncertainties.

It appears that the main Virgo cluster (cluster A), cloud E and the background cloud W are in near-Hubble flow (the deviation of cloud M can be assessed with low significance with only four distance measurements). Cluster B lies at significantly larger distance than predicted from its velocity if it was in Hubble flow. Thus it is falling into Virgo from the far side at ~ -760 km s^{-1}. The two structures N and S have distances similar to the main cluster. However, their velocities are smaller and larger respectively than those of galaxies in dynamic equilibrium with the main body of the Virgo cluster. Cloud N, falling from the far side, and cloud S, falling from the near side, have reached the distance of the main cluster. We remark that these clouds are composed almost entirely of spirals (spiral fraction $\sim$80 per cent), while in all other regions the fraction of these galaxies is $\sim$50 per cent.

The derived parameters of the individual clouds can be compared with similar determinations carried out by previous investigators. Yasuda et al. (1997) found $30.7 < \mu_0 < 31.5$ for cluster A, $\mu_0 \sim 31.7$ for cluster B and $32.4 < \mu_0 < 33.0$ for clouds W and M, in good agreement with ours. However, these authors claim evidence of infall of clouds W and M, which we do not confirm. Federspiel et al. (1998) found $\mu_0 = 31.35$ for cluster A, larger than our estimate, and $\mu_0 \sim 31.81$ for cluster B, in excellent agreement with the present determination.

5.4 The mass estimate of the Virgo cluster

Determining the mass of the Virgo cluster is beyond the scope of the present investigation (see Tully & Shaya 1984 for a comprehensive analysis). However, a simple consistency check can be done by comparing the virial mass of the cluster with the mass required to perturb the Hubble flow in the vicinity of Virgo in order to produce the peculiar velocities observed in the various Virgo clouds and in the Local Group.

The virial mass $M_{\rm vir}$ of the Virgo cluster was estimated by Tully & Shaya (1984) to lie at $\sim 10^{15}$ M$_\odot$ (assuming $H_0 = 80$ km s^{-1} Mpc^{-1}).

The mass required to perturb the Hubble flow expansion can be estimated from $\delta v/v = \Omega^{0.6}/3 \times \delta\rho/\rho$, valid in spherical geometry for density enhancements over the mean density of the Universe $\delta\rho/\rho \sim 1$ (linear regime) (Davis & Peebles 1983). For larger density enhancements (quasi-linear regime) we use the analytic correction scheme proposed by Nusser et al. (1991) (see their equation 34). The deviations from the Hubble flow due to the Virgo cluster at the distance of the Local Group, of cluster B, and of clouds N and W are respectively: $\delta v/v = 220/1354$, 762/701, 768/56 and 150/1236. These correspond to density enhancement $\delta\rho/\rho \sim 1.0$, 6.7, 85 and 0.75 respectively, assuming $\Omega = 0.3$. Clearly large corrections for non-linear regime are required for clouds N and B. Using $\rho = 2 \times 10^{-29}$, and given the distance of 15 Mpc from the Local Group to Virgo, of 8.6 Mpc from cluster B to A, of 0.7 Mpc from cloud N to A, and of 15 Mpc from cloud W to A, the resulting mass enhancement ΔM due to the Virgo cluster ranges between 2.1 and 3.1×10^{15} M$_\odot$. Not surprisingly, this is a factor of 2–3 larger than the virial expectation. In fact, a significant fraction of the mass is

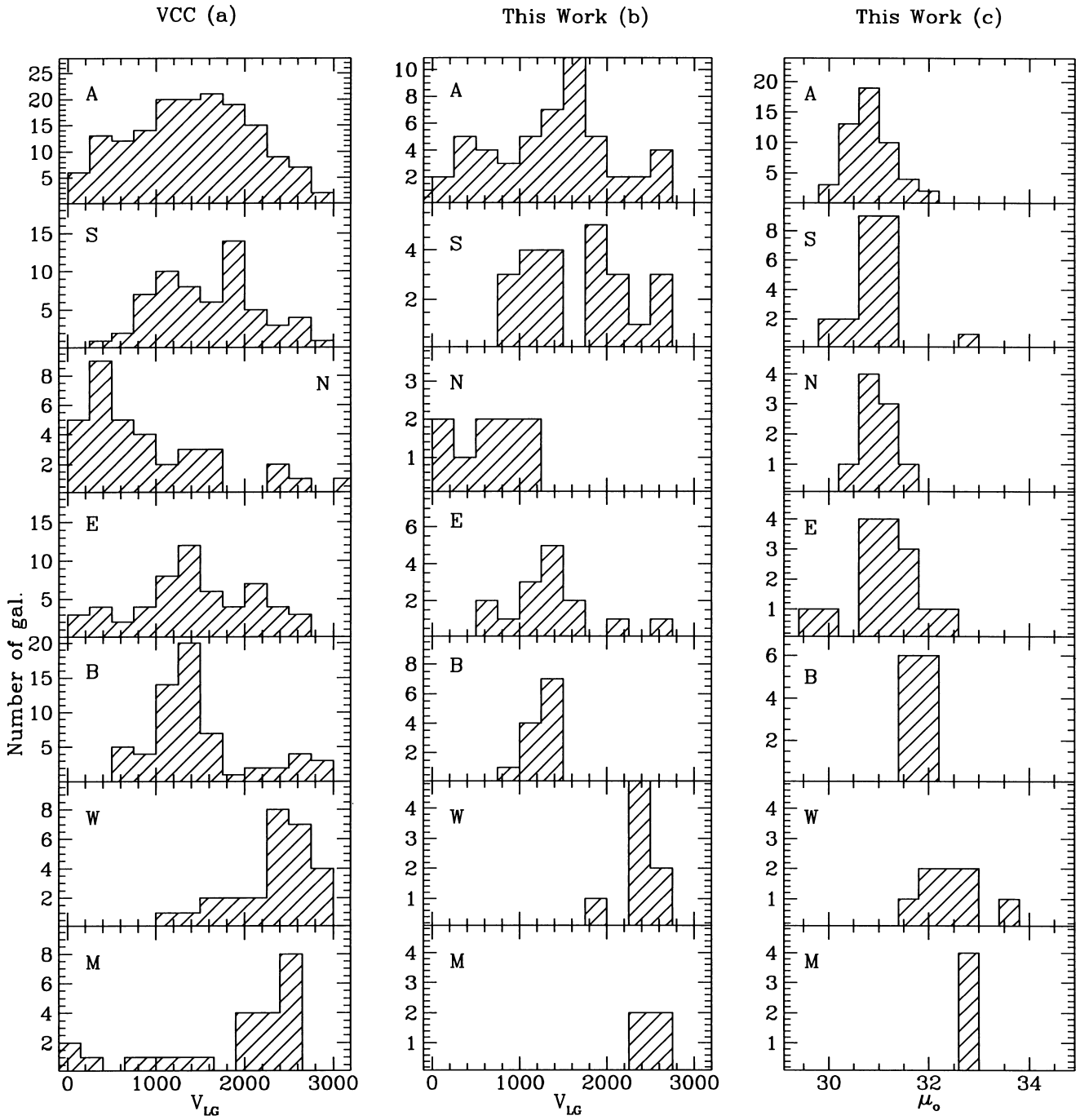

Figure 9. Histograms of V_{LG} in the seven cluster regions: (a) using 433 velocities in the VCC; (b) using 134 galaxies with distance estimates obtained in this work; (c) histograms of the distance moduli obtained in this work in the seven regions of revised membership.

expected to lie outside the main cluster, given the complex structure of Virgo, a structure that is far from being a single, dynamically relaxed entity.

6 SUMMARY AND CONCLUSIONS

We have carried out an *H*-band surface photometry survey of 200 galaxies in the Virgo cluster brighter than $B < 14.0$ mag. These data, complemented with dynamical measurements taken from the literature and with new spectroscopic data for 19 objects, allowed us to derive distances to 134 galaxies in this cluster with either the TF or the FP methods. The individual distance uncertainties are estimated as ∼0.35 and 0.45 mag, for the TF and FP methods respectively.

The Virgo cluster is confirmed to be anything but a virialized cluster. Its main potential well (cluster A) coincides in position with M87, as marked by the distribution of the extended hot gas. An equal mixture of E+S0 and of very H I-deficient spiral galaxies populates this cluster. The cluster appears elongated in the north–south direction. The accuracy of the present distance determinations is still not sufficient to assess convincingly the possible extension in depth.

Table 4. Derived parameters of the Virgo clouds.

Cloud (1)	N_{VCC} (2)	V_{LG} (3)	± (4)	σ_v (5)	± (6)	N_{us} (7)	V_{LG} (8)	± (9)	μ_0 (10)	± (11)	$Vpec_A$ (12)	± (13)
Virgo A	166	1354	54	762	35	51	1369	108	30.84	0.06	0	66
A TF	–	–	–	–	–	28	1315	200	30.83	0.09	–	–
A TF_{def}	–	–	–	–	–	14	1180	480	30.80	0.20	–	–
A TF_{nodef}	–	–	–	–	–	14	1442	235	30.82	0.10	–	–
A FP	–	–	–	–	–	23	1388	91	30.86	0.08	–	–
Cloud N	35	642	121	653	89	9	659	157	30.94	0.12	−768	126
Cloud S	62	1595	75	607	43	23	1677	140	30.91	0.10	+202	105
Cloud E	58	1466	88	702	56	15	1304	90	31.23	0.16	−124	139
Virgo B	62	1293	74	507	55	12	1282	51	31.84	0.10	−762	95
Cloud M	23	2333	173	666	126	4	2507	85	32.77	0.11	(−736)	210
Cloud W	27	2439	94	437	75	8	2435	83	32.38	0.23	−151	275

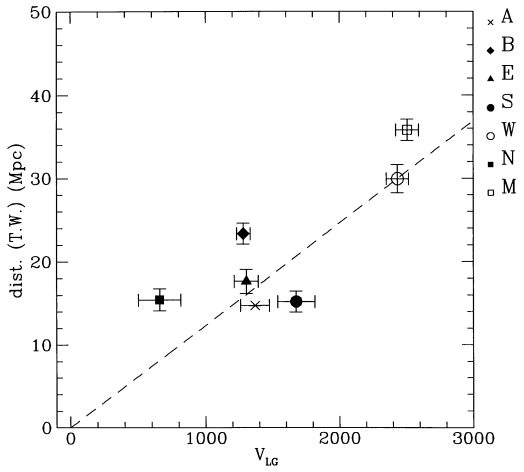

Figure 10. The average distances obtained in this work plotted against the average V_{LG} for each of the seven regions. Error bars indicate 1σ statistical uncertainties on the measured quantities. The broken line represents the Hubble flow, for $H_0 = 81.35$ km s^{-1} Mpc^{-1}.

The second major galaxy aggregate, cluster B, is found to have a smaller spatial extension than originally proposed by Binggeli et al. (1985), and it lies 1 mag further away than Virgo, falling on to the main cluster with -760 km s^{-1} peculiar velocity. M49, projected on to cluster B, is found at significantely smaller distance than B, and thus it is proposed to belong to cloud S. It remains unexplored whether the hot gas found in this region is associated with M49 or with cluster B itself.

Two other clouds, almost exclusively composed of spiral galaxies, are falling on to the cluster (they are at the same distance as A): the one on the north-west is falling from behind (with a peculiar velocity of -768 km s^{-1}), and the other, to the south of A, is falling from the near side at about $+200$ km s^{-1}. None of these galaxies suffers from severe H I deficiency, indicating that the phenomenon has only recently (less than a few $\times 10^8$ yr, the time-scale for gas depletion) taken place (see also Tully & Shaya 1984). Two more galaxy clouds, M and W, projected on the western edge of Virgo, have distances consistent with cluster B. W is in near-Hubble flow, while the velocity of M indicates infall. However, its deviation from the Hubble expansion can be assessed with low statistical significance.

The mass of the Virgo cluster inferred from the peculiar motions induced on its surroundings (Local Group, clouds N, B and W) ranges between 2 and 3×10^{15} $M_\odot$, a factor of 2–3 larger than the virial expectation.

We conclude with a note of caution: owing to the large gravitational perturbation induced by cluster A, galaxies with large peculiar velocities (regions B, N and S) must be cautiously rejected to obtain an unbiased determination of the Hubble constant in the Virgo region. Moreover, N4639, whose $\mu_0 = 32.00$ from the present work coincides with the Cepheids distance obtained with the *HST*, should not be used to represent the distance of Virgo: in fact it belongs to a region (E), containing other galaxies with similarly large distances.

ACKNOWLEDGMENTS

The work reported in this paper was based on observations taken at TIRGO, Gornergrat, Switzerland, at the Calar Alto Observatory, and at the Observatoire de Haute Provence (CNRS), France. TIRGO is operated by CAISMI-CNR, Arcetri, Firenze, Italy. Calar Alto is operated by the Max-Planck-Institut fur Astronomie (Heidelberg) jointly with the Spanish National Commission for Astronomy.

We thank Bruno Binggeli for sending us the VCC in electronic form. We are grateful to the TACs of the TIRGO and Calar Alto Observatories for generous time allocation to this project. We thank C. Baffa, A. Borriello, V. Calamai, B. Catinella, I. Randone, P. Ranfagni, M. Sozzi and P. Strambio for assistance during the observations at TIRGO. Special thanks go to V. Gavriusev for software assistance at TIRGO, and to T. Beers for permission to use his ROSTAT Fortran code. We also wish to thank an unknown referee whose criticism helped to improve this work.

REFERENCES

Ajhar E., Lauer T., Tonry J., Blakesleg J., Bressler A., Holtzman J., Postman M., 1997, AJ, 114, 626
Beers T. C., Flynn K., Gebhardt K. 1990, AJ, 100, 32
Binggeli B., Sandage A., Tammann G., 1985, AJ, 90, 1681 (VCC)
Binggeli B., Popescu C., Tammann G., 1993, A&AS, 98, 275
Böhringer H., Briel U. G., Schwarz R. A., Voges W., Hartner G., Trumper J. 1994, Nat, 368, 828
Boselli A., Casoli F., Lequeux J., 1995, A&AS, 110, 521
Boselli A., Tuffs R., Gavazzi G., Hippelein H., Pierini D., 1997, A&AS, 121, 507
Bottinelli L., Gouguenheim L., Fouque P., Paturel G., 1990, A&AS, 82, 391
Cayatte V., van Gorkom J., Balkowski C., Kotanyi C., 1990, AJ, 100, 604
Chincarini G., de Souza R., 1985, A&A, 153, 218
Ciardullo R., Jacoby G., Feldmeier J., Bartlett R., 1998, ApJ, 492, 62
Davis M., Peebles P., 1983, ARA&A, 21, 109

Della Valle M., Livio M., 1995, ApJ, 452, 704
de Vaucouleurs G., 1948, Ann. Astrophys., 11, 247
de Vaucouleurs G., 1961, ApJS, 6, 213
Djorgovski G., Davis M., 1987, ApJ, 313, 59
Dressler A., 1987, ApJ, 317, 1
Dressler A., Lynden-Bell D., Burstein D., Davies R., Faber S., Terlevich R., Wegner G., 1987, ApJ, 313, 42
Efron B. 1987, J. Am. Stat. Assoc., 82, 171
Elias J., Frogel J., Matthews K., Neugebauer G., 1982, AJ, 87, 1029
Federspiel M., Tammann G., Sandage A., 1998, ApJ, 495, 115
Ferrarese L., Freedman W., Hill R. et al., 1996a, ApJ, 464, 568
Ferrarese L., Livio M., Freedman W., Saha A., Stetson P., Ford H., Hill R., Madove B., 1996b, ApJ, 468, L95
Fukugita M., Okamura S., Yasuda N. 1993, ApJ, 412, L13
Gavazzi G., Boselli A., 1996, Astrophys. Lett. Commun., 35, 1
Gavazzi G., Pierini D., Baffa C., Lisi F., Hunt L., Boselli A., 1996a, A&AS, 120, 521.
Gavazzi G., Pierini D., Boselli A., 1996b, A&A, 312, 397
Giovanardi C., Krumm N., Salpeter E., 1983, AJ, 88, 1719
Giovanelli R., Haynes M., Herter T., Vogt N., da Costa L., Freudling W., Salzer J., Wegner G., 1997, AJ, 113, 53
Haynes M., Giovanelli R., 1984, AJ, 89, 758
Haynes M., Giovanelli R., 1986, ApJ, 306, 466
Helou G., Giovanardi C., Salpeter E., Krumm N., 1981, ApJS, 46, 267
Helou G., Hoffman L., Salpeter E., 1984, ApJS, 55, 433
Herbst T., Beckwith S., Birk C., Hippler S., McCaughrean M., Mannucci F., Wolf J., 1993, SPIE, 1946, 605
Hoffman L., Helou G., Salpeter E., Glosson J., Sandage A., 1987, ApJS, 63, 247
Hoffman L., Lewis M., Helou G., Salpeter E., Williams B., 1989a, ApJS, 69, 65
Hoffman L., Williams H., Salpeter E., Sandage A., Binggeli B., 1989b, ApJS, 71, 701
Hoffman L., Salpeter E., Farhat B., Roos T., Williams H., Helou G., 1996, ApJS, 105, 296
Hutchtmeier W., Richter O., 1986, A&AS, 64, 111
Jacoby G., Ciardullo R., Ford H., 1990, ApJ, 356, 332
Jensen J., Luppino G., Tonry J., 1996, ApJ, 468, 519
Jørgensen I., Franx M., Kjærgaard P., 1996, MNRAS, 280, 167
Kenney J., Young. J., 1988, ApJS, 66, 261
Kenney J., Rubin V., Planesas P., Young J., 1995, ApJ, 438, 135
Lemaitre G., Kohler D., Lacroix D., Meunier J., Vin A., 1990, A&A, 228, 540
Lisi F., Baffa C., Hunt L. K., 1993, SPIE, 1495, 594
Lisi F., Baffa C., Biliotti V. et al., 1996, PASP, 108, 364
McElroy D., 1995, ApJS, 100, 105
Morris P., Shanks T., 1998, MNRAS, 298, 451
Nusser A., Dekel A., Bertschinger E., Blumenthal G., 1991, ApJ, 379, 6
Pahre M., Djorgovski G., de Carvalho R., 1995, ApJ, 453, L17
Peterson S., 1979, ApJS, 40, 527
Pierce M., McClure R., Racine R., 1992, ApJ, 393, 523
Pierce M., Welch D., Mcclure R., van den Bergh S., Racine R., Stetson P., 1994, Nat, 371, 385
Pierce M. J., Tully R. B., 1988, ApJ, 330, 579
Press W., Teukolsky S., Vetterling W., Flannery B., 1992, Numerical Recipes, 2nd edn. Cambridge Univ. Press, Cambridge
Saglia R., Bertschinger E., Baggley G., Burstein D., Colless M., Davies R., McMahan R., Wegner G., 1993, MNRAS, 264, 961
Saha A., Sandage A., Labhardt L., Tammann G., Macchetto F., Panagia N., 1997, ApJ, 486, 1
Sandage A., Saha A., Tammann G., Labhardt L., Panagia N., Macchetto F., 1996, ApJ, 460, L15
Schank T., 1997, MNRAS, 290, L77
Schmidt B., Kirshner R., Eastman R., Phillips M., Suntzeff N., Hamuy H., Maza J., Ariles R., 1994, ApJ, 432, 42
Schneider S., Thuan T., Magri C., Wadiak J., 1990 ApJS, 72, 245
Scodeggio M., 1997, PhD Thesis, Cornell Univ.
Scodeggio M., Giovanelli R., Haynes M., 1997, AJ, 113, 101
Scodeggio M., Gavazzi G., Belsole E., Pierini D., Boselli A., 1998a, MNRAS, 301, 1001
Scodeggio M., Giovanelli R., Haynes M., 1998b, AJ, 116, 2738
Secker J., Harris W., 1993, AJ, 105, 1358
Speraindio M., Chincarini G., Rampazzo R., Molinari E., 1995, A&AS, 110, 279
Sulentic J., Arp H., 1982, AJ, 88, 489
Thronson H., Tacconi L., Kenney J., Greenhouse M., Margulis M., Tacconi-Garman L., Young J., 1989, ApJ, 344, 747
Tonry J., Davis. M., 1979, AJ, 84, 1511
Tonry J., Ajhar E., Luppino G. 1990, AJ, 100, 1416
Trinchieri G., Kim, D.-W. Fabbiano G., Canizares C., 1994, ApJ, 428, 555
Tukey J., 1958, Ann. Math. Stat., 29, 614
Tully B., Fisher R., 1977, A&A, 54, 661
Tully B., Shaya E., 1984, ApJ, 281, 31
van den Bergh S., 1996, PASP, 108, 1091
Warmels R., 1986, Phd thesis, Univ. Groningen
Whitmore B., Sparks W., Lucas R., Biretta J., 1995, ApJ, 454, L73
Yasuda N., Fukugita M., Okamura S., 1997, ApJS, 108, 417
Zwicky F., Herzog E., Karpoviwicz M., Kowal C., Wild P., 1961–68, Catalogue of Galaxies and Clusters of Galaxies. California Institute of Technology, Pasadena (CGCG)

This paper has been typeset from a T_EX/L^AT_EX file prepared by the author.